A Compact Photoacoustic Detector for Trace Acetylene Based on 3-D-Printed Differential Helmholtz Resonators

Fupeng Wang, Liyan Fu, Jinghua Wu, Jianguo Zhang, and Qiang Wang

***Abstract*—Photoacoustic cell is an essential core component in a photoacoustic spectroscopy (PAS) gas sensing system, which is used to enhance and measure the absorption-induced acoustic signal. For certain applications, miniaturized photoacoustic cells with tiny inner volumes are preferred to reduce gas consumption. In this article, a photoacoustic cell with inner volume of only 0.5 mL is designed based on differential Helmholtz resonators (DHRs). After an initial simulation stage by the finite element analysis (FEA) based on COMSOL software, the photoacoustic cell is fabricated by 3-D printing. To facilitate laser power coupling, a micro fiber collimator is customized and integrated with photoacoustic cell to guide the laser beam. New concept of photoacoustic detector is proposed and integrated to a PAS system for trace acetylene detection. As a result, an excellent linearity of 0.99999 is achieved in the concentration range of 0–5000 ppm. A 1σ sensitivity of 0.13 ppm is measured within a response time of 10 s, the minimum detection limit (MDL) is evaluated to be 0.3 ppm. Allan deviation analysis indicate that the detection sensitivity can be improved to 16.6 ppb at an integration time of 910 s.**

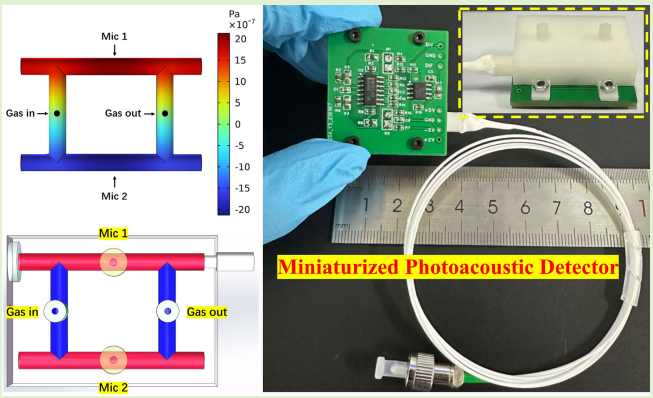

***Index Terms*—3-D printing, Helmholtz resonator, miniaturization, photoacoustic spectroscopy (PAS), trace gas sensor.**

I. Introduction

TRACE gas detection plays an important role across a broad range of applications in atmospheric monitoring, industrial process control, combustion analysis, detection of toxic, explosive gases, as well as medical diagnostics [1], [2]. Recently with the continuous development, optical absorption spectroscopy has been widely used to realize gas detection due to its high selectivity and sensitivity, such as tunable diode laser absorption spectroscopy (TDLAS) [3], [4], cavity ringdown spectroscopy (CRDS) [5], [6], photoacoustic spectroscopy (PAS) [7], [8], [9], [10], [11], [12], [13], photothermal spectroscopy (PTS) [14], [15], [16], [17], and so on. As an indirect absorption spectroscopy technique, PAS has been developed rapidly in recent decades considering its advantages of high sensitivity, high selectivity, and zero background. In addition, PAS system usually uses a microphone or quartz tuning fork (QTF) to measure the absorption-induced acoustic signal to retrieve the gas concentration, instead of a photodetector. Thus, it breaks free from the limitations of light wavelength on photodetectors, making the PAS system can operate in a wide band from visible light, infrared region to terahertz band as long as the light source is available [18]. Another

Manuscript received 15 September 2023; revised 6 October 2023; accepted 6 October 2023. Date of publication 16 October 2023; date of current version 14 November 2023. This work was supported in part by the National Natural Science Foundation of China under Grant 52001295, Grant 62005267, and Grant 62375262; in part by the Natural Science Foundation of Shandong Province under Grant ZR2020QF097; and in part by the Open Fund of State Key Laboratory of Applied Optics under Grant SKLAO2021001A12. The associate editor coordinating the review of this article and approving it for publication was Prof. Santosh Kumar. *(Corresponding author: Fupeng Wang.)*

Fupeng Wang is with the Faculty of Information Science and Engineering, Engineering Research Center of Advanced Marine Physical Instruments and Equipment (Ministry of Education), Optics and Optoelectronics Laboratory (Qingdao Key Laboratory), Ocean University of China, Qingdao 266100, China, and also with the State Key Laboratory of Applied Optics, Changchun Institute of Optics, Fine Mechanics and Physics, Chinese Academy of Sciences, Changchun 130033, China (e-mail: wfp@ouc.edu.cn).

Liyan Fu, Jinghua Wu, and Jianguo Zhang are with the Faculty of Information Science and Engineering, Engineering Research Center of Advanced Marine Physical Instruments and Equipment (Ministry of Education), Optics and Optoelectronics Laboratory (Qingdao Key Laboratory), Ocean University of China, Qingdao 266100, China.

Qiang Wang is with the State Key Laboratory of Applied Optics, Changchun Institute of Optics, Fine Mechanics and Physics, Chinese Academy of Sciences, Changchun 130033, China.

Digital Object Identifier 10.1109/JSEN.2023.3323320

unique characteristic of PAS technique is that photoacoustic signal is proportional to the excitation optical power so that high-power laser can directly increase the photoacoustic excitation. It is also worthwhile to note that PAS is a baseline-free technique where the absorbed energy is measured, rather than the strong transmitted radiation background as in the direct absorption spectroscopy (DAS) system, which means the dynamic range of amplifier circuits can be fully exploited. Thus, the influence of shot noise, flicker noise, and unwanted optical fringe interferences can be avoided [19]. However, the more attractive feature to us is that the PAS technique greatly decreases the dependence on the optical absorption path length in DAS technology. This allows us to design miniaturized gas cells with a short absorption path-length, meanwhile achieve an excellent detection limit by high-power light sources. In some application scenarios requiring trace sample detection, the PAS technique has been employed due to such unique advantage of low gas consumption, such as the dissolved gas measurement [20], [21], [22] and breath analysis [23]. For example, a T-type resonant photoacoustic cell with volume of 30 mL was reported recently to measure the dissolved acetylene gas in oil [24]. The inner volume can be further reduced to milliliter or sub-milliliter level if non-resonant mode is used to design the photoacoustic cell [25], [26]. In such a situation, a high-sensitive cantilever-enhanced optical microphone is usually preferred which is very complicated in manufacturing and signal demodulation. In addition to the electric microphone and optical cantilever, the QTF was also used to measure the absorption signal based on photoacoustic and photothermal effect in the quartz-enhanced PAS (QEPAS) [27] and light-induced thermoelastic spectroscopy (LITES) [28], [29], [30] systems. The QTF is not only small in size, but also has a high resonance frequency which is beneficial for designing very shot acoustic resonators to realize standing wave. As a result of the tiny dimension of QTF and resonators, the photoacoustic cell volume can be easily reduced to a milliliter level. For example, Lin et al. developed a near-infrared (NIR) QEPAS sensor based on a 28 kHz QTF, in which the QTF, acoustic micro resonator, gas cell, and laser fiber were integrated within a super compact space [31]. Afterward in 2023, Zhao et al. developed a sub-mL photoacoustic gas sensor based on QEPAS to measure the dissolved CH_4 at the Haima Cold Spring Area in the South China Sea [22]. An inner size of $12 \times 6 \times 4$ mm was achieved to reduce the total gas consumption to less than 0.3 mL. Although QEPAS has the absolute advantage in miniaturizing the gas cell, however, bare QTF is easily affected by factors such as condensation of water vapor, dust, and corrosion from acid samples, as a result, the long-term stability would be deteriorated [32]. To give a brief summary, the photoacoustic cell does not only provide a place where the laser beam interacts with gas molecules for photoacoustic excitation, but also acts as a loudspeaker for photoacoustic enhancement. Specific geometric design of photoacoustic cell can enhance the acoustic strength in specific frequency. Meanwhile, the inner volume needs to be reduced by optimizing the geometric dimension for trace gas consumption. So, the photoacoustic cells are usually fabricated in a tiny size. As a result, the optical alignment and microphone installation become challenging in such small size. Based on this, we would like to propose a new concept called photoacoustic detector which integrates the optical coupling, photoacoustic cell, microphone or QTF, and differential circuit together in a small size. It would be very compact and easy-to-use for PAS-based applications.

TABLE I
TECHNICAL INDEX REQUIREMENTS FOR TRANSFORMER OIL DISSOLVED ACETYLENE DETECTION

Object	Detection range	Precision Level A	Precision Level B	Precision Level C
C_2H_2	0 ~ 10 ppm	0.5 ppm	1 ppm	3 ppm
	10 ~ 5000 ppm	15%	20%	30%

The degassing volume is estimated to ~ 20 mL, so the gas consumption of developed gas sensor should be less than 20 mL, and less is better.

In this study, we aim to develop a high-sensitivity acetylene sensor with characteristics of low gas consumption for transformer oil application. Table I gives a series of technical index requirements from the end-user. The PAS technique is chosen as our technical proposal due to its properties of low gas consumption and zero background. To ensure the long-term stability of the PAS-based sensor, the electric microphone is chosen to measure the photoacoustic signal because its stability has been verified in the consumer electronics industry. As to the type of photoacoustic cell, a differential Helmholtz resonator (DHR) is adopted because of its absence of a buffer room which can significantly reduce the inner volume of the gas cell. In addition, the differential structure can effectively improve the signal-to-noise ratio (SNR) for photoacoustic detection.

The rest of this study is organized as follows. Section II introduces the detailed design process of the miniaturized photoacoustic module, including the acoustic field simulation, 3-D modeling, and module integration. Section III demonstrates the experiment setup. Section IV presents the experimental results for acetylene detection and gives an analysis. In the end, Section V concludes the study.

II. DESIGN OF MINIATURIZED PHOTOACOUSTIC DETECTOR

A. Acoustic Field Simulation of DHR

Finite element analysis (FEA) was performed to simulate the acoustic field distribution inside the DHR via COMSOL software, the thermoviscous acoustics module was adopted in the simulation whereby both viscous and thermal surface loss were considered to attain accurate simulation results. Furthermore, the mesh close to the boundaries was refined to 0.3 mm. In total, 47 499 mesh elements are generated with a maximum size of 2.4 mm and a minimum size of 0.3 mm. As to the boundary condition, the DHR walls are totally reflected in the acoustic wave which means no tangential component of the acoustic velocity exists. The temperature boundary condition of the DHR walls is set to be isothermal with internal gas. An absorption-induced heat source was positioned along the resonator center with a Gaussian distribution of

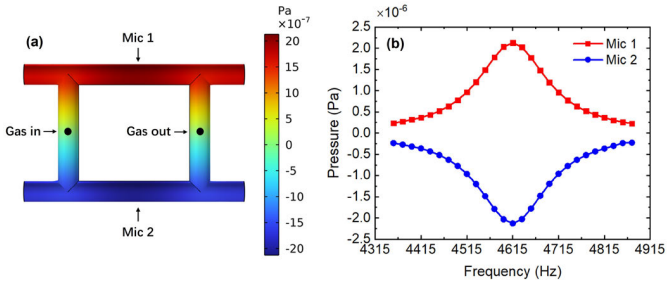

Fig. 1. FEM simulation results of the DHR. (a) Acoustic field distribution at the resonant frequency and (b) sound pressure frequency response of two resonators.

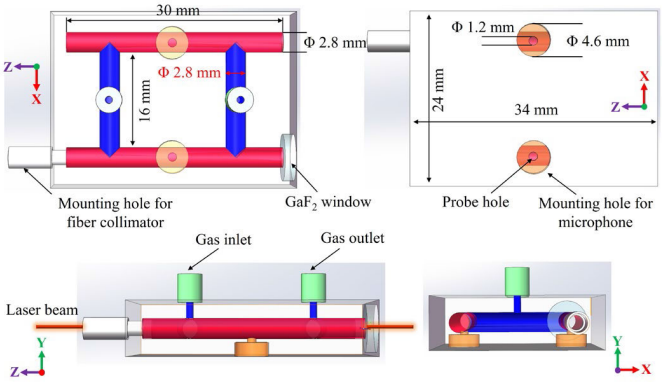

Fig. 2. Different views of the DHR 3-D model designed by SolidWorks software, red color indicates the acoustic resonators, blue color indicates the linking tubes, green color indicates the gas inlet and outlet holes, and yellow color indicates the locations for microphone installation.

0.348 W/m^3. The simulated acoustic field inside the DHR is displayed in Fig. 1, the DHR has a fully symmetrical configuration, composed of two identical cylinders served as acoustic resonators and two tubes to link the resonators. A large amount of optimization was performed to reduce the dimensions of two resonators and tubes so that the inner volume of DHR can be compressed. At last, the lengths of two resonators and two tubes were set at 30 and 16 mm respectively, their diameters were both 2.8 mm, resulting in ~0.5 mL inner volume. The acoustic field distribution at resonant frequency is depicted in Fig. 1(a). In this resonance mode, the antinodes of the acoustic waves are in the middle of two resonators and the maximum sound pressure is 2.15×10^{-6} Pa based on simulation. Furthermore, as illustrated in Fig. 1(b), the frequency response of the DHR was calculated, according to which the resonant frequency was determined to be 4616 Hz and the full width at half maximum (FWHM) of frequency response curve was obtained to be 313 Hz, resulting in a Q-factor of 14.7.

B. Three-Dimensional Modeling of DHR

Based on the simulation results, the inner dimension of the DHR was determined. Afterward, a 3-D model was designed by SolidWorks software as shown in Fig. 2, overall dimension of the DHR cell is 34 × 24 mm. A mounting hole was set at the end of one resonator so that a micro fiber collimator can directly insert into the resonator for coupling laser beam, the other end was a CaF_2 window in diameter of 6 mm for optical power monitoring. Another resonator was closed at both ends. Gas inlet and outlet holes were located at the middle of two linking tubes with an inner diameter of 1 mm. Two microphones were installed at the middle of two acoustic resonators to detect the acoustic signal. The diameters of mounting hole and probe hole were 4.6 and 1.2 mm respectively, which was related to the microphone's size and its sensitive surface. After that the 3-D model was finished, the DHR cell was 3-D-printed with material of white resin in a precision of ±0.1 mm.

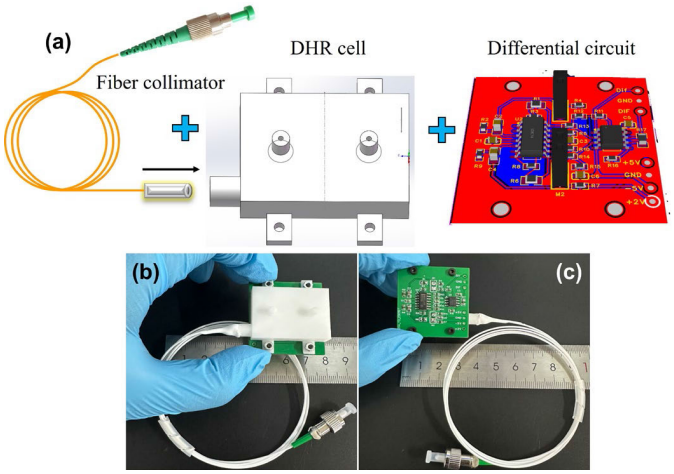

Fig. 3. (a) Photoacoustic detector assembly diagram. (b) and (c) Take pictures on the developed photoacoustic detector.

C. Photoacoustic Detector Integration

One of the highlights of this study is that we developed a compact photoacoustic detector, which can be easily applied to any PAS-based system for gas detection. The photoacoustic detector was realized by integrating a microfiber collimator, a DHR cell, and a mini differential circuit together as shown in Fig. 3(a). A micro fiber collimator operating at 1531 nm was customized for this study, it can provide a laser beam with a diameter <1 mm in 80 mm working distance. The collimator head was inserted in the mounting hole of DHR cell and reinforced with the silicon rubber. A mini circuit board was designed by ourselves for differential detection, which was mounted with the DHR cell by four screw holes. As a result, a so-called photoacoustic detector was achieved as displayed in Fig. 3(b) and (c). The concept of photoacoustic detector is like the widely used photodetector. For example, in a photoelectric system, photodetector is necessary and used to convert the optical signal into electrical current. Similarly, the proposed photoacoustic detector in a PAS system is also used to convert the optical signal into electrical voltage as well. You do not need to pay attention to the process of optical alignment, photoacoustic excitation, photoacoustic detection, and so on. You just need to connect the photoacoustic detector as shown in Fig. 4 to a probe laser by a FC/APC fiber connector, and measure its output voltage for absorption-induced harmonic demodulation. The detailed specification indicators are listed in Table II.

TABLE II
DESIGN INDICATORS OF THE PA DETECTOR

Operating wavelength	1531 nm
Insert loss	0.37 dB
Transmitted laser beam diameter	< 1 mm
Fiber connector	FC/APC
Resonance center frequency	4616 Hz
FWHM	313 Hz
Power supply	DC: ±5 V to ± 18 V
Gain bandwidth product	11 MHz
Optional gain	0dB, 20dB, 34dB, 40dB or customized
Output mode	Differential analog output
Electrical connector	2.54 mm Header or Soldering
Pressure	Atmospheric pressure
Sample gas flow rate	⩽ 350 sccm

sccm: standard cubic centimeter per minute.

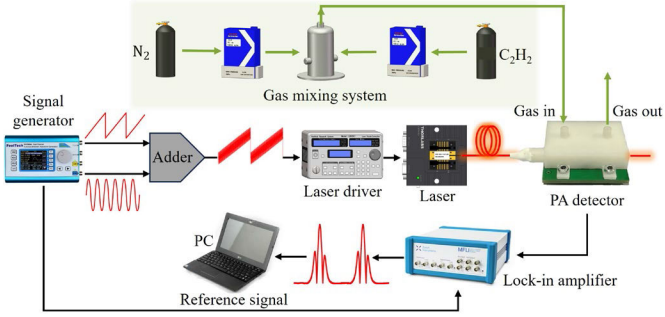

Fig. 4. Schematic of experiment setup.

III. EXPERIMENT SYSTEM SETUP

An experiment system was set up as shown in Fig. 4 to test the developed photoacoustic detector for acetylene detection. A DFB laser operating at 1531 nm was used to select the C_2H_2 absorption line at 1531.58 nm (6529.17 cm^{-1}), where the molecular absorption line strength is 1.16 × 10^{-20} $cm^{-1}/(molec \cdot cm^{-2})$. The laser temperature was stabilized at 27.5 °C by a commercial laser driver (LDC501, Stanford Research Systems, USA). Sawtooth wave in frequency of 0.1 Hz and sine wave in high frequency f were generated and added to drive the DFB laser by the LDC501 as well. The sinusoidal signal in the same frequency of f was also generated and connected to a lock-in amplifier (MFLI, Zurich Instrument, Zurich, Switzerland) as a reference. The DFB laser output was coupled into the photoacoustic detector by a FC/APC fiber connector. The voltage signal from the photoacoustic detector was connected to the lock-in amplifier for second harmonic detection, the gain of the photoacoustic detector was set to 40 dB, and the bandwidth of the eight-order lowpass filter of the MFLI was set 1 Hz to reduce noise interference in the following experiments. A LabVIEW-based program was performed on a personal computer to save the second harmonic signals and calculate the amplitudes. Sample

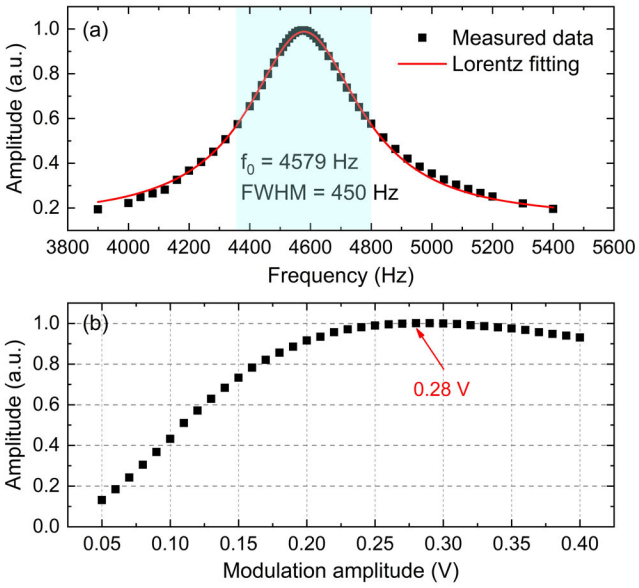

Fig. 5. (a) Measured frequency response curve of DHR and (b) wavelength modulation amplitude optimization results. FWHM: full width at half maximum.

acetylene in different concentrations was provided by a gas mixing system, including two flowmeters, 0.5% C_2H_2 and 99.999% pure nitrogen. All the experiments were carried out at room temperature and atmospheric pressure.

IV. EXPERIMENT RESULTS

A. Parameters Optimization

The frequency response of the DHR has been simulated in Fig. 1(b), the first step of our experiment is to measure the realistic resonance frequency of the 3-D-printed DHR. In the experiment, a C_2H_2 sample in concentration of 5000 ppm was introduced into the DHR cell for photoacoustic excitation. Among the absorption-induced harmonics, the second harmonic signal was chosen and measured in this study to infer the gas concentration. So, the laser modulation frequency f was changed from 1950 to 2700 Hz (half of the DHR resonance frequency) and the absorption-induced second harmonic amplitudes were measured and normalized as shown in Fig. 5(a). The results indicate that the fabricated DHR has a center frequency of 4579 Hz, which is slightly different from the simulated result of 4616 Hz. Nonlinear fitting utilizing a Lorentzian profile was performed on the frequency response data, the FWHM was measured to be 450 Hz, resulting in a Q-factor of 10.2. The difference between experiment and simulated results may arise from fabrication error and test conditions.

Given that the wavelength modulation spectroscopy (WMS) technique was adopted in the PAS system, an optimization experiment was carried out to determine the optimal modulation amplitude for the DFB laser. The measured second harmonic amplitudes versus different modulation amplitudes are plotted in Fig. 5(b), the second harmonic amplitude increases as the modulation amplitude (sine wave amplitude) increases. At last, the amplitude of the sinusoidal modulation signal is measured to be 0.28 V to achieve a maximum second

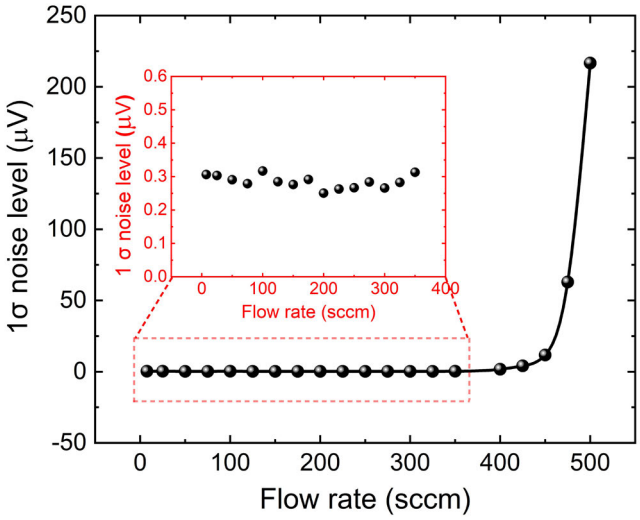

Fig. 6. Influence of different gas flow rates on noise level.

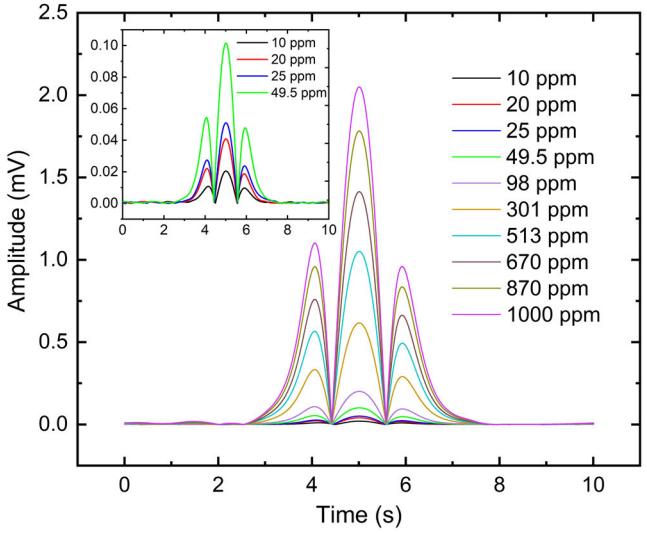

Fig. 7. Displayed second harmonic signals in different acetylene concentration from 10 to 1000 ppm range.

harmonic signal. Thus, the optimized modulation amplitude was determined and used in the following experiments.

Considering that there was no gas buffer chamber specially designed for the DHR cell in this study, excessive airflow may disturb the sound pressure field in the resonators and introduce additional noise. So, the experiment was carried out to study the influence of different gas flow rates on noise levels. In the experiment, 5000 ppm C_2H_2 was imported to the DHR cell in different flow rates from 7.5 to 500 sccm, meanwhile the 1σ standard deviation was calculated based on the non-absorption baseline of the second harmonic signal to represent the noise. As shown in Fig. 6, the noise level does not change when the flow rate is below 350 sccm, and then increases. When the gas flow is set larger than 450 sccm, the background noise increases rapidly. Thus, the total flow rate was controlled under 350 sccm in the following experiments.

B. Acetylene Concentration Detection

After the experiments of parameters optimization, the key parameters of the experiment system were fixed, including the sawtooth scanning frequency (0.1 Hz), wavelength modulation frequency (2290 Hz), lowpass bandwidth of lock-in amplifier (eight-order, 1 Hz), and laser modulation amplitude (0.28 V). Afterward, sample C_2H_2 in different concentrations from 10 to 5000 ppm was provided by the gas mixing system for the gas detection test. The measured second harmonic curves below 1000 ppm were displayed in Fig. 7, to make the curves in low concentrations easier for observation, the second harmonic curves of 10, 20, 25, and 49.5 ppm were zoomed out as an inset in Fig. 7. Afterward, the second harmonic amplitudes were measured and plotted in Fig. 8, based on which linear fitting was performed to achieve an efficiency of 2.05 μV/ppm with an R^2 of 0.99999.

To evaluate the potential sensitivity for acetylene detection, a long-term experiment of 2 h was carried out, during which the acetylene sample in concentration of 20 ppm was provided for measurement and the second harmonic amplitudes were measured and saved at a sampling rate of one data point

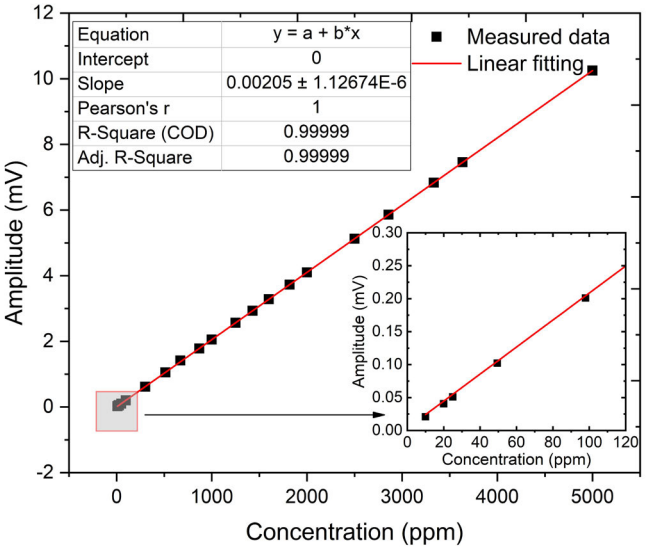

Fig. 8. Linear fitting in a concentration range of 0–5000 ppm.

per 10 s. Afterward, the measured amplitudes in voltage unit were converted into concentration unit based on the linear equation in Fig. 8 and plotted in Fig. 9(a). Statistical analysis was carried out on the data, a 1σ sensitivity of 0.17 ppm was achieved in a response time of 10 s. Considering that Allan deviation was usually used to analyze the long-term stability and determine the main sources of noise for a sensing system, it can provide information about the optimal integration time for averaging and allow the prediction of the best detection sensitivity or detection limit. So, the Allan deviation analysis has been widely applied to PAS-based gas sensors to explore the potential performance for concentration detection [33], [34]. In this study, the Allan deviation analysis was also applied to the 2-h-measured data to evaluate the potential sensitivity when we increased the integration time, the result was displayed in Fig. 9(b). The detection sensitivity could be improved to 58.2 ppb if the integration time was extended to

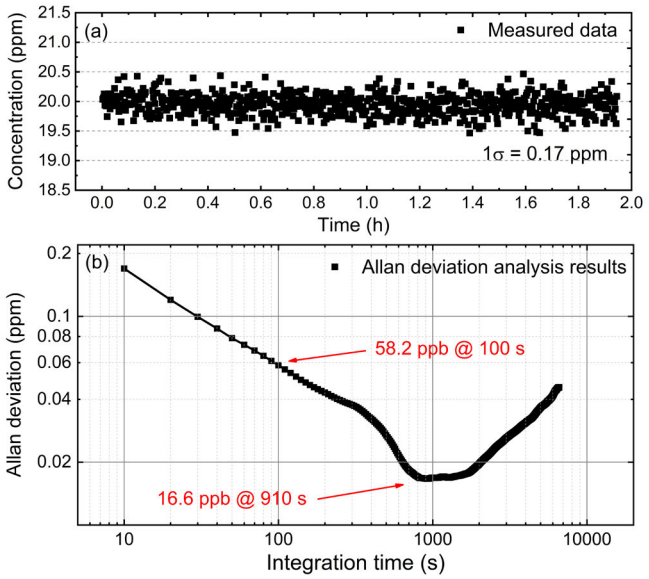

Fig. 9. Allan deviation analysis to evaluate the sensitivity. (a) Long-term measured results of 20 ppm acetylene for ~2 h. (b) Allan deviation analysis results.

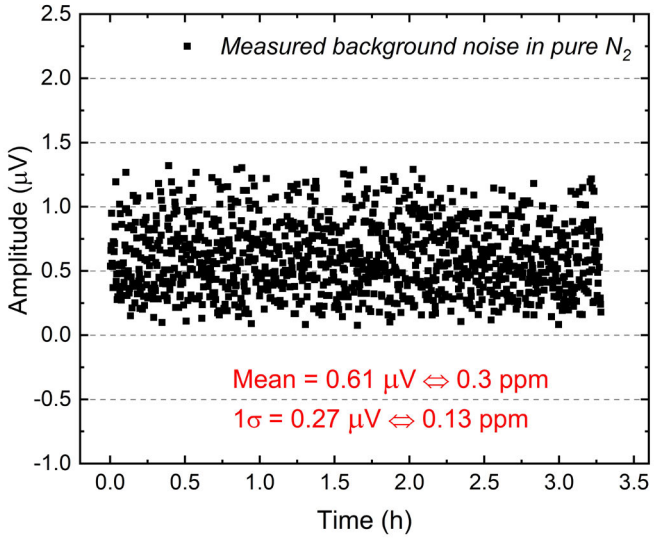

Fig. 10. MDL analysis for acetylene detection, non-absorption background measured in 99.999% nitrogen.

100 s, and to 16.6 ppb if the integration time was extended to 910 s.

To estimate the minimum detection limit (MDL) of the developed photoacoustic sensor for acetylene detection, the second harmonic amplitudes were continuously measured in 99.999% nitrogen over 3 h as plotted in Fig. 10. The statistical analysis was performed on the measured data to calculate the mean value, and use the mean value to represent the non-absorption background of the photoacoustic sensor. Results in Fig. 10 shows that the background is 0.61 μV which cannot be reduced any more by increasing the integration time. Furthermore, we repeatedly measured the background for several times which indicated that the mean value was very stable at 0.61 μV. This means any absorption-induced second harmonic amplitude below 0.61 μV cannot be identified any more. We substituted 0.61 μV into the linear fit equation in Fig. 8, the MDL was determined to be 0.3 ppm. The 1σ detection sensitivity was calculated to be 0.13 ppm in the pure nitrogen environment, which was a litter better than the result displayed in Fig. 9(a). The reason may be that the gas mixing system introduces additional uncertainty when providing the 20 ppm sample acetylene, which was not the business of the photoacoustic sensor itself. So, we think the detection sensitivity of 0.13 ppm at a response time of 10 s is more convincing.

To give a brief summary, the concept of a photoacoustic detector was proposed by combining the optical coupling, photoacoustic cell, and differential circuit together. In other words, it was an attempt to the direction of high integration for more convenient applications in engineering. Researchers from the University Grenoble Alpes also did a series of such studies on downsizing the photoacoustic trace gas sensors. Three generations of components, namely a 40 mm^3 3-D-printed cell, a 3.7 mm^3 silicon cell, and a 2.3 mm^3 silicon cell with a built-in piezoresistive pressure sensor, had been designed [35]. All three versions of photoacoustic cells have their own domain of operation as each one has benefits and drawbacks, regarding fabrication, implementation, and ease of use. We share the same viewpoint that MEMS ON chip is a very promising direction for the field of PAS-based gas detection. In addition, photonic crystal fiber (PCF) has been developed rapidly in recent years and used to develop various PCF-based sensors which also have the characteristic of mini size [36], [37], [38], [39], [40]. For gas detection, the hollow-core fiber is also employed as the gas chamber in DAS [41] and PTS [42] systems to reduce the volume of gas consumption. In such applications, the fiber only provides a micro cavity for interaction between light and gas molecular, the optical coupling and photodetector are still separated. Compared with the above studies, we take a step forward by adding the parts of optical coupling and differential detection to the photoacoustic module instead of only designing the photoacoustic cell (gas cell) itself. It is true that such design increases the dimension of the entire module. However, it becomes easier for integration to our opinion. That is why we design the photoacoustic detector as a fiber coupled one. Of course, there are still challenges on the path of miniaturizing the photoacoustic module, one of which is the additional noise induced by gas flow as reported in Section IV-A. To deal with such problem, some buffer structures should be designed as well when optimizing the photoacoustic cell. As to the parameters of detection sensitivity and MDL, they have met the requirements of the technical indicators in Table I. The next step is the further integration of the whole experiment system as depicted in Fig. 4 for field test.

V. Conclusion

We developed a miniaturized photoacoustic cell DHR with tiny inner volume of only 0.5 mL to improve the response speed for trace gas detection, especially for conditions of dissolved gas measurement. By virtue of the 3-D printing

technology, the PA cell can be easily fabricated. Moreover, a new concept of photoacoustic detector was proposed by integrating the fiber collimator, photoacoustic cell and differential circuit together, which was very compact and easy-to-use for engineering application. Based on the photoacoustic detector, a miniaturized photoacoustic sensor for acetylene measurement was validated, the best sensitivity of 16.6 ppb and MDL of 0.3 ppm were achieved in acetylene detection experiment. After further integration, it would be applied to measure the dissolved trace gas in transformer oil. In the next step, effort will be made to further miniaturizing the DHR and differential circuit to make the photoacoustic detector more like a sensor chip.

REFERENCES

[1] M. Gu et al., "Open-path anti-pollution multi-pass cell-based TDLAS sensor for the online measurement of atmospheric H_2O and CO_2 fluxes," *Opt. Exp.*, vol. 30, no. 24, pp. 43961–43972, 2022.

[2] H. Tai, S. Wang, Z. Duan, and Y. Jiang, "Evolution of breath analysis based on humidity and gas sensors: Potential and challenges," *Sens. Actuator B, Chem.*, vol. 318, Sep. 2020, Art. no. 128104.

[3] L. Dong et al., "Compact TDLAS based sensor design using interband cascade lasers for mid-IR trace gas sensing," *Opt. Exp.*, vol. 24, no. 6, pp. A528–A535, Mar. 2016.

[4] F. Wang, J. Chang, Q. Wang, W. Wei, and Z. Qin, "TDLAS gas sensing system utilizing fiber reflector based round-trip structure: Double absorption path-length, residual amplitude modulation removal," *Sens. Actuators A, Phys.*, vol. 259, pp. 152–159, Jun. 2017.

[5] A. Maity, S. Maithani, and M. Pradhan, "Cavity ring-down spectroscopy: Recent technological advancements, techniques, and applications," *Anal. Chem.*, vol. 93, no. 1, pp. 388–416, Jan. 2021.

[6] D. Lisak et al., "Dual-comb cavity ring-down spectroscopy," *Sci. Rep.*, vol. 12, no. 1, p. 2377, Feb. 2022.

[7] T. Tomberg, M. Vainio, T. Hieta, and L. Halonen, "Sub-parts-per-trillion level sensitivity in trace gas detection by cantilever-enhanced photoacoustic spectroscopy," *Sci. Rep.*, vol. 8, no. 1, p. 1848, Jan. 2018.

[8] F. Wang et al., "Techniques to enhance the photoacoustic signal for trace gas sensing: A review," *Sens. Actuators A, Phys.*, vol. 345, Oct. 2022, Art. no. 113807.

[9] A. A. Kosterev, Y. A. Bakhirkin, R. F. Curl, and F. K. Tittel, "Quartz-enhanced photoacoustic spectroscopy," *Opt. Lett.*, vol. 27, no. 21, pp. 1902–1904, 2002.

[10] H. Wu et al., "Beat frequency quartz-enhanced photoacoustic spectroscopy for fast and calibration-free continuous trace-gas monitoring," *Nature Commun.*, vol. 8, no. 1, p. 15331, May 2017.

[11] Z. Li, J. Liu, G. Si, Z. Ning, and Y. Fang, "Design of a high-sensitivity differential Helmholtz photoacoustic cell and its application in methane detection," *Opt. Exp.*, vol. 30, no. 16, pp. 28984–28996, 2022.

[12] C. Zhang, S. Qiao, Y. He, S. Zhou, L. Qi, and Y. Ma, "Differential quartz-enhanced photoacoustic spectroscopy," *Appl. Phys. Lett.*, vol. 122, no. 24, Jun. 2023, Art. no. 241103.

[13] Z. Li, J. Liu, G. Si, Z. Ning, and Y. Fang, "Active noise reduction for a differential Helmholtz photoacoustic sensor excited by an intensity-modulated light source," *Opt. Exp.*, vol. 31, no. 2, pp. 1154–1166, 2023.

[14] Q. Wang et al., "Dual-comb photothermal spectroscopy," *Nature Commun.*, vol. 13, no. 1, p. 2181, Apr. 2022.

[15] D. Pinto et al., "Parts-per-billion detection of carbon monoxide: A comparison between quartz-enhanced photoacoustic and photothermal spectroscopy," *Photoacoustics*, vol. 22, Jun. 2021, Art. no. 100244.

[16] P. Zhao et al., "Mode-phase-difference photothermal spectroscopy for gas detection with an anti-resonant hollow-core optical fiber," *Nature Commun.*, vol. 11, no. 1, p. 847, Feb. 2020.

[17] C. Yao, S. Gao, Y. Wang, W. Jin, and W. Ren, "Heterodyne interferometric photothermal spectroscopy for gas detection in a hollow-core fiber," *Sens. Actuator B, Chem.*, vol. 346, Nov. 2021, Art. no. 130528.

[18] S. Borri et al., "Terahertz quartz enhanced photo-acoustic sensor," *Appl. Phys. Lett.*, vol. 103, no. 2, Jul. 2013, Art. no. 021105.

[19] P. Werle, "Accuracy and precision of laser spectrometers for trace gas sensing in the presence of optical fringes and atmospheric turbulence," *Appl. Phys. B, Lasers Opt.*, vol. 102, no. 2, pp. 313–329, Feb. 2011.

[20] C. Li et al., "High-sensitivity dynamic analysis of dissolved gas in oil based on differential photoacoustic cell," *Opt. Lasers Eng.*, vol. 161, Feb. 2023, Art. no. 107394.

[21] K. Chen et al., "Detection of ultra-low concentration acetylene gas dissolved in oil based on fiber-optic photoacoustic sensing," *Opt. Laser Technol.*, vol. 154, Oct. 2022, Art. no. 108299.

[22] H. Zhao et al., "A fiber-coupled quartz-enhanced photoacoustic sensor for dissolved gas detection," *Photonics*, vol. 10, no. 2, p. 127, Jan. 2023.

[23] N. Maurin et al., "First clinical evaluation of a quartz enhanced photoacoustic CO sensor for human breath analysis," *Sens. Actuators B, Chem.*, vol. 319, Sep. 2020, Art. no. 128247.

[24] G. Wang et al., "Rapid detection of dissolved acetylene in oil based on T-type photoacoustic cell," *Microw. Opt. Technol. Lett.*, pp. 1–7, Jun. 2023, doi: 10.1002/mop.33793.

[25] L. Fu et al., "Small-volume highly-sensitive all-optical gas sensor using non-resonant photoacoustic spectroscopy with dual silicon cantilever optical microphones," *Photoacoustics*, vol. 27, Sep. 2022, Art. no. 100382.

[26] G. Wu et al., "High-sensitivity multitrace gas simultaneous detection based on an all-optical miniaturized photoacoustic sensor," *Anal. Chem.*, vol. 94, no. 36, pp. 12507–12513, Sep. 2022.

[27] F. Wang et al., "Wavelength scanning Q-switched fiber-ring laser intra-cavity QEPAS using a standard 32.76 kHz quartz tuning fork for acetylene detection," *Opt. Laser Technol.*, vol. 134, Feb. 2021, Art. no. 106612.

[28] Y. Ma, T. Liang, S. Qiao, X. Liu, and Z. Lang, "Highly sensitive and fast hydrogen detection based on light-induced thermoelastic spectroscopy," *Ultrafast Sci.*, vol. 3, p. 24, Jan. 2023.

[29] W. Chen et al., "Hollow-waveguide-based light-induced thermoelastic spectroscopy sensing," *Opt. Lett.*, vol. 48, no. 15, pp. 3989–3992, 2023.

[30] Z. Lang, S. Qiao, and Y. Ma, "Fabry–Pérot-based phase demodulation of heterodyne light-induced thermoelastic spectroscopy," *Light, Adv. Manuf.*, vol. 4, no. 2, p. 23, 2023.

[31] Y. Liu et al., "Integrated near-infrared QEPAS sensor based on a 28 kHz quartz tuning fork for online monitoring of CO_2 in the greenhouse," *Photoacoustics*, vol. 25, Mar. 2022, Art. no. 100332.

[32] F. Wang, J. Chang, Q. Zhang, Z. Qin, and C. Zhu, "Pivotal techniques evaluation in QEPAS system for engineering applications," *Measurement*, vol. 135, pp. 376–384, Mar. 2019.

[33] M. Giglio, P. Patimisco, A. Sampaolo, G. Scamarcio, F. K. Tittel, and V. Spagnolo, "Allan deviation plot as a tool for quartz-enhanced photoacoustic sensors noise analysis," *IEEE Trans. Ultrason., Ferroelectr., Freq. Control*, vol. 63, no. 4, pp. 555–560, Apr. 2016.

[34] F. Wang, J. Wu, Y. Cheng, L. Fu, J. Zhang, and Q. Wang, "Simultaneous detection of greenhouse gases CH_4 and CO_2 based on a dual differential photoacoustic spectroscopy system," *Opt. Exp.*, vol. 31, no. 21, pp. 33898–33913, 2023.

[35] A. Glière et al., "Downsizing and silicon integration of photoacoustic gas cells," *Int. J. Thermophys.*, vol. 41, no. 2, Feb. 2020, Art. no. 16.

[36] V. S. Chaudhary, D. Kumar, B. P. Pandey, and S. Kumar, "Advances in photonic crystal fiber-based sensor for detection of physical and biochemical parameters—A review," *IEEE Sensors J.*, vol. 23, no. 2, pp. 1012–1023, Jan. 2023.

[37] V. S. Chaudhary, D. Kumar, and S. Kumar, "Au-TiO_2 coated photonic crystal fiber based SPR refractometric sensor for detection of cancerous cells," *IEEE Trans. Nanobiosci.*, vol. 22, no. 3, pp. 562–569, Jul. 2023.

[38] G. P. Mishra, D. Kumar, V. S. Chaudhary, and S. Kumar, "Design and sensitivity improvement of microstructured-core photonic crystal fiber based sensor for methane and hydrogen fluoride detection," *IEEE Sensors J.*, vol. 22, no. 2, pp. 1265–1272, Jan. 2022.

[39] X. Liu et al., "Feasibility analysis of an SMS-/MSM-/SMSMS-based optical fiber sensor structure," *Appl. Opt.*, vol. 61, no. 9, pp. 2327–2332, Mar. 2022.

[40] V. S. Chaudhary, D. Kumar, and S. Kumar, "SPR-assisted photonic crystal fiber-based dual-wavelength single polarizing filter with improved performance," *IEEE Trans. Plasma Sci.*, vol. 49, no. 12, pp. 3803–3810, Dec. 2021.

[41] Z. Zhang et al., "Seconds-scale response sensor for in situ oceanic carbon dioxide detection," *Anal. Chem.*, vol. 95, no. 7, pp. 3577–3586, Feb. 2023.

[42] M. Hu, C. Yao, A. Ventura, J. G. Hayashi, F. Poletti, and W. Ren, "Mid-infrared photothermal gas sensor enabled by core-cladding mode interference in a hollow-core fiber," *J. Lightw. Technol.*, vol. 40, no. 19, pp. 6568–6575, Oct. 1, 2022.

Fupeng Wang received the Ph.D. degree in optical engineering from Shandong University, Jinan, China, and the University of Washington, Seattle, WA, USA, in 2019.

He is currently an Assistant Professor with the Ocean University of China, Qingdao, China. His research interests include tunable laser absorption spectroscopy (TDLAS), photoacoustic spectroscopy (PAS), nondispersive infrared spectroscopy (NDIR), and spectroscopy-based engineering applications in ocean detection and atmosphere analysis.

Liyan Fu was born in Heze, China, in 1999. She received the bachelor's degree in software engineering from Lyuliang University, Lvliang, China, in 2022. She is currently pursuing the master's degree with the Engineering Research Center of Advanced Marine Physical Instruments and Equipment (Ministry of Education), Ocean University of China, Qingdao, China.

Her research interests include photoacoustic spectroscopy (PAS) and miniatured integration for dissolved gas detection.

Jinghua Wu was born in Dezhou, Shandong, China, in 1999. He received the bachelor's degree in optoelectronic information science and engineering from the Nanyang Institute of Technology, Nanyang, China, in 2021.

He is engaged in the nondispersive infrared (NDIR) sensor, photoacoustic spectroscopy (PAS) sensor development, and application for ocean detection.

Jianguo Zhang was born in Jining, Shandong, China, in 1999. He received the bachelor's degree in optoelectronic information science and engineering from the Nanyang Institute of Technology, Nanyang, China, in 2022.

His research interests include spectral overlap analysis, development of field programmable gate array (FPGA), and engineering application of trace gas detection.

Qiang Wang received the B.S. degree in electronic science and technology and the Ph.D. degree in optical engineering from Shandong University, Jinan, China, in 2011 and 2016, respectively.

After his graduate study, he worked as a Postdoctoral Fellow at the Chinese University of Hong Kong, Hong Kong, and the Max Planck Institute of Quantum Optics, Munich, Germany. He is currently a Full Professor with the State Key Laboratory of Applied Optics, Changchun Institute of Optics, Fine Mechanics and Physics, Chinese Academy of Sciences, Changchun, China. His recent research interests include laser spectroscopy, optical sensing, and engineering application of trace gas analysis in the atmosphere, deep sea, and public health.